# 15

# INORGANIC CAPSULES: REDOX-ACTIVE GUESTS IN METAL CAGES

ANDREW MACDONELL AND LEROY CRONIN

## 15.1 INTRODUCTION

Inorganic capsules can be considered as both an offshoot of and an alternative to their organic counterparts. Whether in pure inorganic assemblies or combined with organic ligands, the versatile coordinations of the transition metals allow for a satisfying variety of architectures and the phenomenon of self-assembly allows complex structures to form in one-pot reactions with near-quantitative yields. Starting with a review of transition metals as components in capsule structures and looking at the development of this field, the focus of this chapter will then shift to polyoxometalates, inorganic molecules composed primarily of transition metals held together by oxygen bridges, giving an introduction to this unique chemical family followed by a discussion regarding how self-assembled architectures can provide an alternative form of encapsulation.

### 15.1.1 Transition Metals in Capsule Formation

A fundamental problem in the synthesis of organic capsules is the complexity of the target molecules. Due to the linear nature of hydrogen bonds, one of the principal intramolecular forces utilized in the design of organic capsules, the curvature of the capsule, has to be introduced elsewhere, which can demand lengthy and complex syntheses [1]. One means of achieving complex architectures without intensive synthetic effort is to make use of the varying coordination geometries of transition metals. By employing rigid polydentate ligands with more than one coordination site, it is possible to direct the self-assembly of complex three-dimensional polyhedral structures, in which the metals act as vertices and the linkers act as edges (with two coordination sites) or faces (with more than two) [2]. Some example structures are shown in Figure 15.1.

The structures produced by this method can be synthesized in one-pot reactions and at near-quantitative yield, although some synthetic effort may be involved in the synthesis of the organic ligands.

A comprehensive overview of transition metal capsules would require more space than this chapter is able to give. However, a general impression of the achievements of the field will be attempted. Two interesting results will be looked at: The first is a capsule functioning as an enzyme mimic which ultimately achieves enzyme-like rate acceleration, and the second is an investigation into the use of crystalline capsules as hosts for reactions.

### 15.1.2 Capsules for Catalysis

The work performed by the Raymond group (supramolecular chemistry) in conjunction with the Bergman group (catalysis) has provided a thorough exploration of a specific capsule system used to catalyze a number of simple organic reactions [3]. The capsule is shown on the left in Figure 15.1 with the formula $[Ga_4L_6]^{12-}$ (L = *N*,*N*′-bis(2,3-hydroxybenzoyl)-1,5-diaminonaphthalene). The naphthalene-based ligands form the edges of the tetrahedral structure, meeting at the four gallium-atom vertices, where three bidentate ligands occupy the octahedral coordination sphere of the gallium. These capsules form without a templating guest, are water-soluble and stable to guest exchange, and provide a hydrophobic cavity of up to 450 Å [3].

*Organic Nanomaterials: Synthesis, Characterization, and Device Applications*, First Edition. Edited by Tomás Torres and Giovanni Bottari.
© 2013 John Wiley & Sons, Inc. Published 2013 by John Wiley & Sons, Inc.

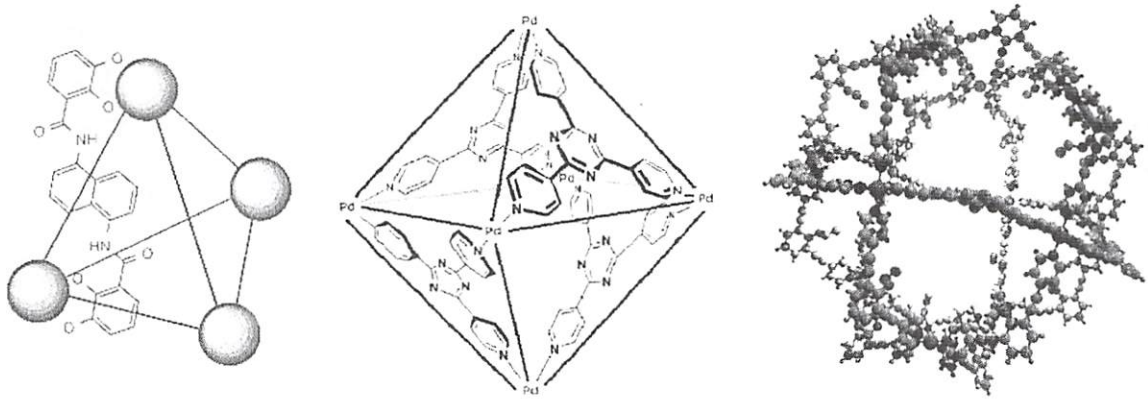

**FIGURE 15.1.** Three transition metal capsules. (**Left**) Gadolinium metal centers with a naphthalene-based linear ligand (Raymond). (**Center**) Palladium metal centers with triazole-based trigonal planar ligands (Fujita). (**Right**) Palladium centers with curved ligands bearing pendant glucose groups (Fujita).

The observation that water-reactive species could be stabilized within the hydrophobic cavity [4] prompted further research into encapsulating protonated guests. This revealed that protonated amines could be preserved inside the capsules even above pH values that would deprotonate a free amine, suggesting a strong stabilization [5]. It was reasoned that these capsules, following from the theory of transition state stabilization in enzyme catalysis [6], could catalyze reactions with protonated transition states in their rate-determining step.

Orthoformate and acetal hydrolysis, the mechanisms of which are shown in Figure 15.2 (both in solution and encapsulated within $Ga_4L_6$), were both investigated as model systems for this catalytic effect.

Both are acid-catalyzed systems and both result in a product with significantly different binding properties to the substrate, which decreases the likelihood of product inhibition and improves turnover. One of the more intuitive measures of catalytic activity is $k_{cat}/k_{uncat}$, which shows how many times faster the catalyzed reaction is compared to the uncatalyzed reaction under the same conditions. For the orthoformate reactions, this increase was between 150 and 3900 times, depending on the shape, size, and hydrophobicity of the compounds [7]. For the two acetal hydrolysis reactions, the increases were 190 and 980 [8]. While these results are a confirmation of the initial theory, the rate accelerations obtained are small compared to enzymatic catalysis [9]. However, using the same system to catalyze a different reaction, the Nazarov cyclization of pentadienols (shown in Figure 15.3 with the additional Diels–Alder step required to overcome the problem of product inhibition), two of the substrates studied showed rate accelerations on the order of $10^6$ ($2.1$ and $1.7 \times 10^6$) [10]. This led the group to suggest that this combination of constrictive binding and functional group activation could be a general strategy for achieving enhanced reactivity.

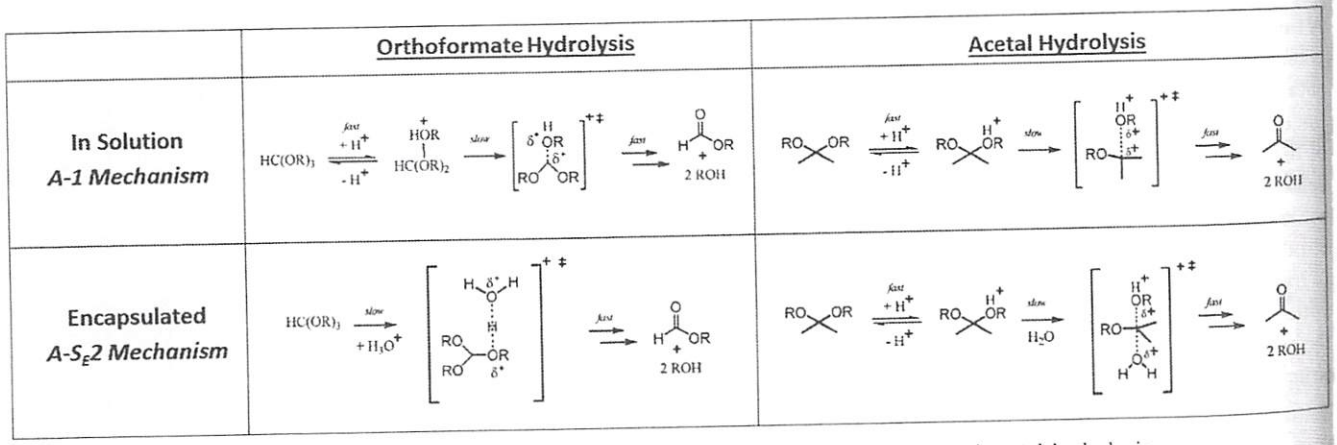


**FIGURE 15.2.** Scheme showing the different mechanisms of orthoformate and acetal hydrolysis both in solution without encapsulation and within the $[Ga_4L_6]^{12-}$ capsule.

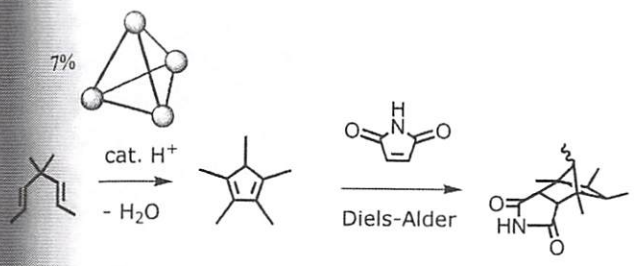


**FIGURE 15.3.** Scheme showing the conditions used for the Nazarov cyclization of Pentadienols, including the Diels–Alder reaction step required to avoid product inhibition.

### 15.1.3 Crystalline Capsules

A novel application of transition metal capsules has been pioneered by the Fujita group, in which they use crystallized molecular capsules to contain reactions, allowing the encapsulated guests to be observed via crystallography. If anything more than the slightest of chemical transformations are attempted on the component molecules of crystalline structures, the associated reorganization of the molecule will disrupt the regular repeating structure of the crystal, leading to an amorphous product [11]. However, if a molecular capsule forms the crystal, reactions can occur within their cavities without influencing the external crystal structure. Fujita's group, as a proof of concept, used an octahedral capsule with alternate closed and open faces formed from square-planar palladium (the vertices) and tris(4-pyridyl)triazine ligands (the faces) [12] as shown in the center of Figure 15.1. This was self-assembled and mixed in solution with acenaphthylene, forming a capsule–(acenapthylene)$_2$ complex from which crystals were formed by slow evaporation of the solvent [13]. While x-ray diffraction showed the acenaphthylene disordered over three positions within the cage, ultraviolet irradiation led to the [2 + 2] photodimerization, with the syn-product observed via x-ray diffraction [14]. A similar system, with encapsulated Cp'Mn(CO)$_3$ undergoing photodissociation of carbonyl ligands, was also investigated, showing that labile and otherwise non-isolable compounds could be clearly observed [15].

## 15.2 POLYOXOMETALATES

In addition to the numerous examples of organic–inorganic capsules available, there is also a family of entirely inorganic molecules which are capable of self-assembling into an astonishingly wide variety of clusters. This family, known as the polyoxometalates, contains a number of subsets capable of functioning as entirely inorganic capsule structures. Polyoxometalates, or POMs as they are commonly known, are discrete inorganic metal oxide molecules. Though their architectures and composition vary greatly, they share some distinguishing common features; they are all composed of high-oxidation-state, early-row transition metals (normally, though not exclusively, Mo and W) linked together by oxygen bridges to form polyhedral units in which the metal defines the center and the oxygen atoms define the vertices. These polyhedral units then link together, by sharing either one, two, or three oxygen vertices, referred to as corner-, edge- and face-sharing, respectively [16]. Depending on the nature of the metals and the reaction conditions, this linking of polyhedral units will lead to any one of a number of complex POM architectures based upon these basic building blocks. The resulting structures may have anywhere between 2 and 368 metal centers, with structures as diverse as wheels, crowns, spheres, and stars (see Figure 15.4) [17].

### 15.2.1 Synthesis and Assembly

POMs are normally assembled by acidifying a solution of the transition metal oxyanion, leading to the self-assembly of a variety of structures depending on specific pH, temperature, and the presence of other reagents. Somewhat surprisingly, despite the ubiquity of POMs in recent publications and the number of research groups regularly working with them, the actual formation mechanism has not been extensively researched. Initial theoretical speculation looking at tungsten POMs suggested that protonated $WO_4$ units would come together directly, followed by dehydration reactions to produce larger assemblies. This process was then elaborated to lead to the formation of larger POMs, despite limited

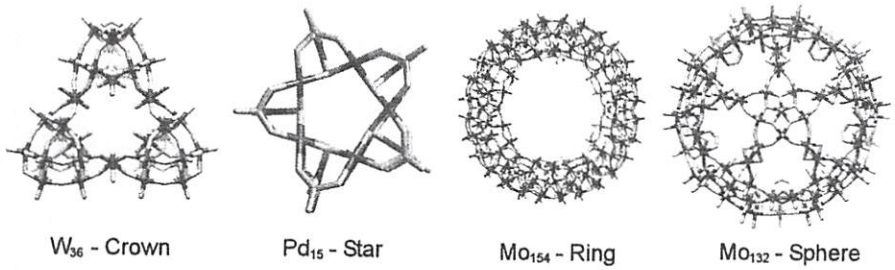


**FIGURE 15.4.** Crystal structures showing the variety of POM architectures, showing the metal, oxygen, and heteroatom components.

experimental evidence [18]. However, recent work employing DFT calculations and ESIMS experiments suggests that this theory does not fit as well as an alternative method, proposing a more complex mechanism of protonation and dimerisation, supported by MS identification of intermediate peaks [19].

In aqueous solution, POMs form at low pH and they require these conditions to remain stable; raising the pH will often cause the POM to degrade. However, raising the pH under strict conditions can cause the selective removal of metal centers, leading to so-called *lacunary* POMs. This *lacuna* can then be filled by a different transition metal, giving a mixed-addenda polyoxoanion, allowing new properties to be imbued and tuned. Lacunary structures can also serve as building blocks for larger POM structures.

### 15.2.2 Isopolyanions and Heteropolyanions

The many structures of polyoxometalates can be divided easily into two principal subgroups: isopolyanions, which are composed purely of metal and oxygen atoms, and heteropolyanions, which are composed of metal and oxygen atoms plus at least one heteroatom. Their formulas may be expressed as follows:

Isopolyanions (**IPAs**): $[M_nO_y]^{p-}$
Heteropolyanions (**HPAs**): $[X_aM_nO_y]^{q-}$, where $a \leq n$

The metal atoms, M, are considered to be peripheral to the heteroatoms and are referred to as *addenda* using Pope's terminology [16]. These addenda atoms are restricted to metals which can form strong d–π p–π bonds with oxygen, but the heteroatoms have no such restriction, with at least 65 elements represented. In the context of polyoxometalates, isopolyoxometalates (*iso*-POMs) and heteropolyoxometalates (*hetero*-POMs) are often used interchangeably with IPAs and HPAs.

The heteroatoms can be further divided into primary ("central") and secondary ("peripheral") heteroatoms. The primary heteroatoms are those which are crucial to the structure, normally (though not always) positioned in the center of the cluster, while the secondary heteroatoms may be removed from the structure to leave an independently stable HPA, an example of which would be the Cr(III) in $[SiW_{11}Cr(H_2O)O_{39}]^{5-}$ which can be removed to give $[Cr(H_2O)]^{3+}$ and $[SiW_{11}O_{39}]^{8-}$. The primary heteroatoms can direct both the chemistry and architecture of the clusters they form part of, with a general formula of $[XO_y]^{n-}$ but normally forming tetrahedral $[MO_4]^{n-}$ structures with M most commonly being Si, Ge, P, As or S. Metallic heteroatoms also occur, such as tetrahedral Co(III) or the $[XO_6]$ found at the center of the Anderson structure $[XM_6O_{24}]^{n-}$, where X = Mn(III), Te(VI), or Ni(II). The most common HPAs, however, are the Keggin and Wells–Dawson structures, which are of particular interest because the primary heteroatoms are entirely encapsulated within the metal cage.

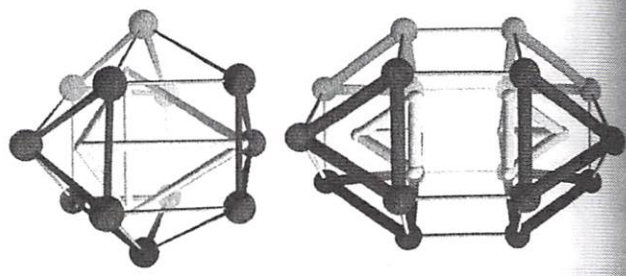

**FIGURE 15.5.** Schematic representation of the structures of the Keggin (**Left**) and Dawson (**right**) clusters. The triangles represent $[M_3O_9]$ units with the gray bonds representing their shared bridging oxygens. The tetrahedrons represent the heteroanions.

### 15.2.3 Keggin and Wells–Dawson Structures

The Keggin $([XM_{12}O_{40}]^{n-}$ is one of the simplest heteropolyanionic structures, with a central heteroatom surrounded by 12 metal centers and 40 oxygen atoms (4 oxygens linking to the heteroatom, 24 bridging between metal centers, and 12 terminal oxo ligands on the metal centers). A simple means of understanding the structure is to consider the 12 metal centers making 4 triangles made of edge-sharing $[M_3O_9]$ units. The heteroatom and its four oxygens form a tetrahedron with a corner in the center of each of the four triangles. These triangles are then linked together at the corners to form a cage, as is shown on the left of Figure 15.5. The Keggin formula can be altered to better represent this structure as $[(XO_4)(M_3O_9)_4]^{n-}$ (all future Keggin–Dawson-based structures will provide this alternative structural formula). The five isomers of this structure are achieved by rotating each of these triangles by 45°. This increases edge-sharing in preference to corner sharing, bringing the metal centers closer together and increasing repulsion, making the isomers progressively less energetically favorable.

Slightly altering the reaction conditions for the Keggin anion can lead to the formation of the Wells–Dawson heteropolyanion $([X_2M_{18}O_{62}]^{n-})$. Its 62 oxygen atoms can be divided into 8 bonding to the heteroatoms, 36 bridging between metal centers, and 18 terminal oxo ligands. Its structure is equivalent to two Keggin clusters, each with one $[M_3O_9]$ triangle unit removed, bound together by six equatorial oxo ligands at the position of the missing triangular units (see Figure 15.5). Similarly to the Keggin structure, its formula can be altered to $[\{(XO_4)(M_3O_9)_3\}_2]^{n-}$. It has six isomers and, for both the Keggin and Dawson structures, the combination of isomerization and lacunary structures can result in exposed oxo ligands attached to the heteroatom, able

to coordinate directly to transition metals, which is of importance in catalysis. Both the Keggin and Dawson structures will be revisited in more detail.

### 15.2.4 Redox-Active Guests

For heteropolyanions possessing exposed heteroatoms, such as in the Anderson structure, these may play a direct role in the molecule's reactivity. However, for the Keggin–Dawson structure the heteroatoms are entirely surrounded by the metal atoms they bond to and they are often referred to as being "encapsulated" within the "cage" of the polyoxometalate framework. Though this prevents them from reacting directly with their chemical environment, there are other means by which the heteroatoms can be active in the chemical properties of the molecule.

One of the distinguishing characteristics of POMs is their ability to accept and donate electrons without significant change to their overall structure. Although POMs usually form with the addenda metal atoms in their highest oxidation state ($d^1$ or $d^0$), they are easily reduced, forming mixed-valence addenda species. Considering that these clusters are made up of many metal centers and that each metal center can potentially accept or donate multiple electrons, it is easy to imagine why POMs have been referred to as "electron reservoirs." If it were proven possible to link the redox potential of the cage with an encapsulated heteroatom functioning as a dopant, it could lead to molecules exhibiting properties not observed in their bulk analogues, which could form part of single-molecule electronic devices. This idea shall be returned to in the discussion of Wells–Dawson clusters.

### 15.2.5 Cation Exchange and Cation-Directed Synthesis

Since POMs are anionic, this charge must be balanced with cations. Normal synthetic conditions typically lead to small alkali metal cations or protons, but these can often be exchanged for bulkier organic equivalents. Cation exchange allows several properties of the POM to be altered or tuned, such as solubility or rate of crystallisation. Recently, however, it has been explored as a means of constructing new POM structures.

The popular "building-block" concept advocates the use of small POM units (building blocks), carefully chosen for their shape and charge, as a means of constructing large, complex clusters through controlled aggregation, as was demonstrated by Müller, who showed that, by varying reaction conditions and using building blocks such as the pentagonal $\{Mo(Mo)_5\}$ unit with suitable linkers, it was possible to construct huge mixed-valence clusters with varied structures, such as the spherical icosohedral $\{Mo_{132}\}$, big wheel $\{Mo_{154}/Mo_{176}\}$, capped cyclic $\{Mo_{248}\}$, and basket-shaped $\{Mo_{116}\}$ architectures [20]. In order to extend this concept,

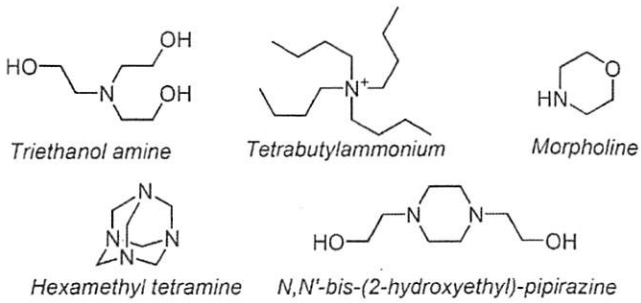


**FIGURE 15.6.** Some of the bulky organic cations used in the "shrink-wrapping" strategy.

a range of suitable low-symmetry clusters (i.e., with high negative charge and high nucleophilicity), such as Müller's pentagonal $\{Mo(Mo)_5\}$ unit, must be made available. However, the basic POM structures tend to be spherical or near-spherical (with high symmetry) in form due to the tendency of these highly charged, potent nucleophiles to aggregate into uniform, stable structures.

The Cronin group at Glasgow University, UK, has investigated a means of preventing this aggregation by a form of "reverse-templating" with bulky organic counterions [21]. It was found that bulky organic amine cations used in synthesis helped to isolate POM species in one-pot reactions, trapping and stabilizing them, thereby preventing their aggregation into more stable clusters and leading not only to novel compounds, but to entirely novel structures. In addition, they can also serve to direct the self-assembly of these building blocks into extended structures [22]. The amines used, shown in Figure 15.6, were primarily hexamethylene tetramine (HMTA/$HMTAH^+$), triethanol amine (TEA/$TEAH^+$), *N,N*-bis-(2-hydroxyethyl)-pipirazine (BHEP/$BHEPH^+$), and morpholine, capable of acting as encapsulating cations in the synthesis, but also functioning as buffers and even redox reagents in some cases. The technique is frequently referred to as "shrink-wrapping," due to the remarkably small distances between the POM surface and the cations, or "inverse templating," comparing it to the role of classical central templates, for example, in the formation of aluminosilicates or aluminophosphates [23].

This technique has led to a wealth of new discoveries. The first cluster to be isolated in this way using ($HMTAH^+$) was an isopolyoxomolybdate, with the formula $(C_6H_{14}N_4)_{10}[H_2Mo_{16}O_{52}]\cdot 34H_2O$. In contrast to other polyoxomolybdates of similar nuclearity, this structure is flat; four of the 12 Mo centers are one-electron reduced and the overall structure of the molecule has a central $Mo_{12}$ cluster, with two $Mo_2$ "wings" extending on either side, as shown in Figure 15.7. The role of "shrink-wrapping" can be seen in the very close interactions between the cluster and the cations: The presence of 18 short hydrogen-bonded, cluster-surface, oxygen-to-cation interactions in the range of 2.581(7)

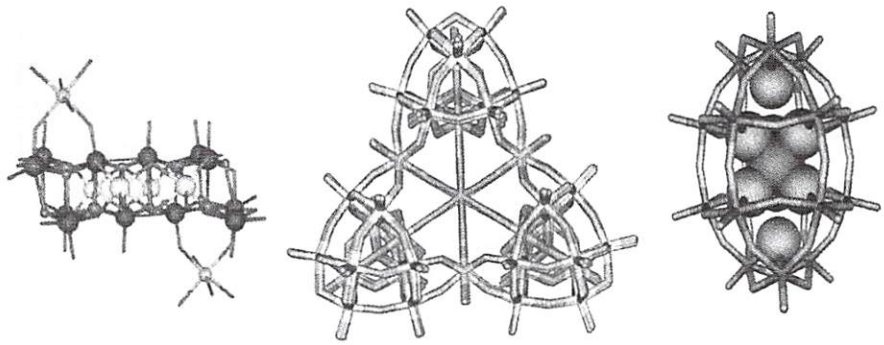

**FIGURE 15.7.** Crystal structures for each of the first three structures to come from the "shrink-wrap" technique. (**Left**) The $[H_2Mo_{16}O_{52}]^{10-}$ "bat-wing" cluster. (**Center**) The $[H_{12}W_{36}O_{120}]^{12-}$ "Celtic ring" cluster. (**Right**) The $[H_4W_{19}O_{62}]^{6+}$ "tungsten-centered Dawson" cluster.

$\leq d$[E(-H)... O(MO)] $\leq$ 3.140(5) Å shows that the cluster and cations are extensively linked via hydrogen bonds [24].

Applying this technique to tungsten systems using ($TEAH^+$) led to the discovery of a new isopolyoxotungstate $[H_{12}W_{36}O_{120}]^{12-}$, $\{W_{36}\}$, composed of three $[H_4W_{11}O_{38}]^{6-}$ units linked together by three $[WO_6]$ bridges to form a ring structure which maps well onto the structure of an 18-crown-6 crown ether, as shown in Figure 15.7. Based on this, the possibility of the central cavity taking part in host–guest chemistry was investigated, resulting in the successful synthesis of several $\{W_{36}\text{-}M\}$ ($M = K^+, Rb^+, Cs^+, NH_4^+, Sr_2^+$ and $Ba^{2+}$) complexes. Further extension to a range of protonated aliphatic and aromatic guests showed not only that they were successfully bound in the cavity, but that the protruding components of these structures, the organic "tail", could direct the formation of the crystalline structures [25].

The next structure to be isolated is more relevant to the topic of inorganic capsules. While still being an isopolyoxometalate, the $(TEAH^+)_6[H_4W_{19}O_{62}]$, $\{W_{19}\}$ cluster has the external structure of a Dawson polyanion with a triangular-prismatic or octahedral (depending on the isomer) $[WO_6]^{6-}$ anion acting as the central template, replacing the normal two tetrahedral heteroanions (see Figure 15.7). The $[WO_6]^{6-}$ anion is positioned in the middle of the cluster, between two $\mu_3$-oxo ligands; and between these oxo ligands and the central anion are two tetrahedral "voids" in the positions usually occupied by the two heteroanions [26].

## 15.3 THE WELLS–DAWSON CLUSTER $[X_2M_{18}O_{62}]^{n-}$

The general structure of the Wells–Dawson cluster has already been mentioned. However, there are several significant variations upon this structure, stemming principally from the encapsulated heteroatoms. In order to fully understand the novelty of these systems, the structure of the classic Dawson must first be revisited in more depth.

As has been mentioned, the Wells–Dawson cluster has the formula $[X_2M_{18}O_{62}]^{n-}$ or $[\{(XO_4)(M_3O_9)_3\}_2]^{n-}$, equivalent to two trilacunary Keggin structures joined symmetrically. The cage formed is generally oval in shape with terminal oxo ligands on the exterior of the cluster extending out from each of the metal centers. The internal structure relies upon the $(XO_4)$ heteroanion template: one $\mu_4$-oxo ligand coordinates to the three metal centers in the "cap" at the narrow end of the oval, while the remaining three $\mu_3$-oxo ligands coordinate to two metal centers in the "belt" portion, at the middle of the oval. There are six possible isomers for the Dawson cage—the first three represent different rotations of the two caps:

| | | |
|---|---|---|
| $\alpha$ | Neither cap rotated | $D_{3h}$ symmetry |
| $\beta$ | One cap rotated | $C_{3v}$ symmetry |
| $\gamma$ | Both caps rotated | $D_{3h}$ symmetry |

For each of these, it is then possible to rotate the molecule around its equator, leading to:

| | | |
|---|---|---|
| $\alpha^*$ | Neither cap rotated | $D_{3h}$ symmetry |
| $\beta^*$ | One cap rotated | $C_{3v}$ symmetry |
| $\gamma^*$ | Both caps rotated | $D_{3h}$ symmetry |

The $\alpha$-isomer is the most common structure followed by the $\gamma^*$, while $\beta$ and $\gamma$ have not yet been observed crystallographically (although their presence has been inferred using other spectroscopic methods [27]) and the $\alpha^*$-isomer has not yet been experimentally observed. In structures with missing or shifted heteroanions (which will be encountered in the following sections), additional oxygen atoms are found on the $(W_3O_9)$ units, forming $(W_3O_{10})$ triangles, where the extra oxygen is located above the center of the triangle and coordinates to the three metal centers, replacing those usually provided by the heteroanion. These extra oxygens are often protonated.

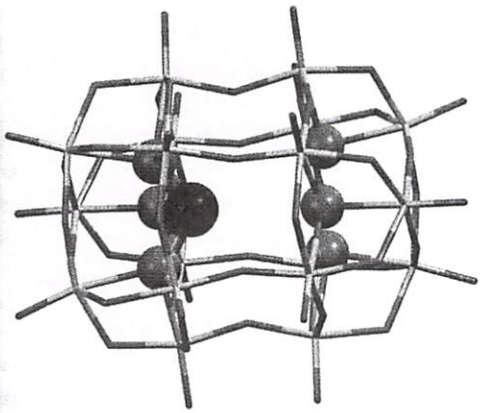

**FIGURE 15.8.** Crystal structure of the $[H_2AsW_{18}O_{60}]^{7-}$ cluster, **1**.

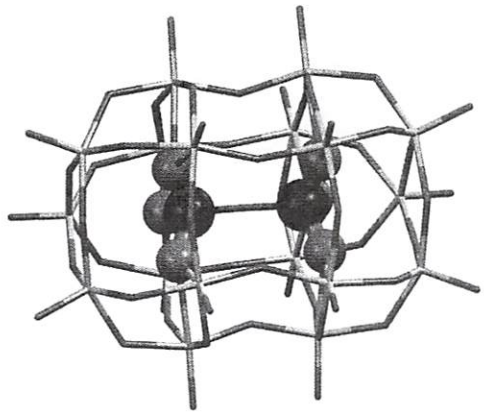

**FIGURE 15.9.** Crystal structure of the $[P_2Mo_{18}O_{61}]^{4-}$ cluster, **2**.

### 15.3.1 Single-Pyramidal Dawson $[H_x(XO_3)M_{18}O_{56}]^{n-}$

A significant difference from the oval-cage and tetrahedral-heteroanion form of the classic Dawson is found for structures incorporating pyramidal heteroanions. These include $[H_2AsW_{18}O_{60}]^{7-}$ (reformulated as $[\{(AsO_3)(W_3O_9)_3\}\{(H_2)(W_3O_{10})_3\}]^{7-}$) [28] (**1**) and $[H_3BiW_{18}O_{60}]^{7-}$ (reformulated as $[\{(BiO_3)(W_3O_9)_3\}\{(H_3)(W_3O_{10})_3\}]^{6-}$) [29] (**2**), both of which contain only one heteroanion, leaving the remaining void to be stabilized by protonated oxygens, in a fashion similar to that of the the Keggin-based metatungstate structure $[H_2W_{12}O_{40}]^{6-}$ ($[(H_2)(W_3O_{10})_4]^{6-}$). The As structure, which is representative of the monopyramidal structures, is depicted in Figure 15.8. Since the lone pairs of the pyramidal heteroatoms point into the center of the cluster, it has been suggested that the electronic repulsion this would generate, given the ionic radii of the heteroatoms, would make it impossible to fit two $AsO_3$ or $BiO_3$ units into the same cluster, providing a reason why they form these single-heteroatom species.

### 15.3.2 Pyrophosphate Dawson $[(P_2O_7)Mo_{18}O_{54}]^{4-}$

The next elaboration of the Dawson structure was synthesized in 1990 by Himeno *et al.* [30] and had its x-ray structure derived in 1994 by Kortz and Pope [31]; the $[P_2Mo_{18}O_{61}]^{4-}$ (or reformulated as $[(P_2O_7)\{(Mo_3O_9)_3\}_2]^{4-}$) (**3**) structure represented a new kind of Dawson structure, in which the two heteroanion positions are filled by a linked pyrophosphate group, as shown in Figure 15.9.

This was significant for a number of reasons: The internal structure of the Dawson is different, with each $\mu_4$-oxo ligand of the pyrophosphate bridging one metal center from the cap and two from the belt; the bond lengths between the Mo atoms of the "caps" and the oxygens of the pyrophosphate groups are unusually long (2.64–2.72 Å), although this is also true (to a lesser extent) of the Keggin and Dawson structures with phosphate heteroanions (~2.4 Å), lending these compounds a more clathrate character; the corner-sharing in preference to edge-sharing which occurs in the "caps" of the pyrophosphate Dawson increases the distance between the Mo centers, which, given that the belt region has a similar size to the regular Dawson structure, gives the overall compound an hourglass or peanut-shaped structure; the pyrophosphate contained within the capsule was the first to be unambiguously assigned as having a linear, eclipsed P–O–P structure, all previous P–O–P structures being either nonlinear or having data which could be otherwise interpreted. Two reduced forms of the cluster were also investigated: the dark green one-electron-reduced compound and the dark blue two-electron-reduced compound, which showed mixed-valence electron mobility (a measure of the temperature at which an electron in a mixed-valent compound becomes "trapped" at a metal center) somewhere between the equivalently reduced phosphate Dawson cluster and phosphate Keggin cluster.

### 15.3.3 Double-Pyramidal Dawson $[(XO_3)_2M_{18}O_{54}]^{6-}$

A further alteration of the classic Dawson was achieved by the Cronin group in 2004, when, using the aforementioned "shrink-wrapping" technique, the two-electron-reduced $[(SO_3)_2Mo_{18}O_{54}]^{6-}$ (reformulated as $[\{(SO_3)(Mo_3O_9)_3\}_2]^{6-}$) (**4a**) was isolated using ($TEAH^+$) as the counterion [32]. This was the first example of the pyramidal $SO_3$ anion acting as a heteroanion in a Dawson structure and, while pyramidal structures have been incorporated into Dawson clusters before, this was also the first example of two non-linked pyramidal heteroanions contained within a Dawson cluster, as can be seen in Figure 15.10.

Both the internal and external structure of the cage is similar to the pyrophosphate Dawson, although the lack of an oxygen bridge between the heteroatoms leads to a slightly tighter $O_6$ "belt" region. Two fully oxidized equivalents

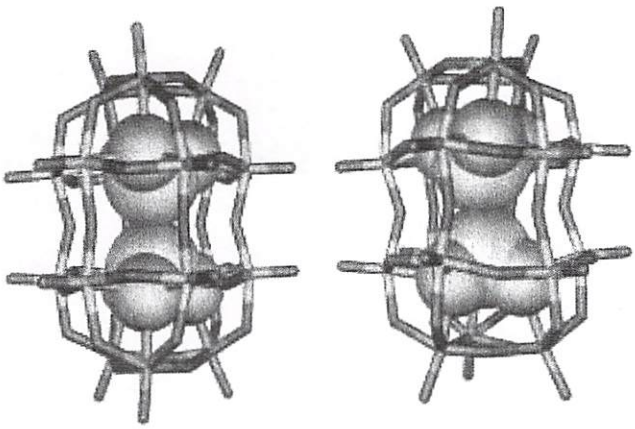

**FIGURE 15.10.** Crystal structure of the sulfite Dawson with the reduced $[\alpha\text{-}(SO_3)_2Mo_{18}O_{54}]^{6-}$ cluster **4a** (**left**) and the fully oxidized $[\beta\text{-}(SO_3)_2Mo_{18}O_{54}]^{4-}$ cluster **4c** (**right**).

were also synthesized, $[(SO_3)_2Mo_{18}O_{54}][Mo_6O_{19}](Bu_4N)_6$ (**4b**) and $[(SO_3)_2Mo_{18}O_{54}](C_2H_3N)(Bu_4N)_4$ (**4c**), in order to better understand the consequences of sulfite encapsulation. Compound **4b** crystallized with the $[Mo_6O_{19}]^{2-}$ Lindqvist anion, while compound **4c** was the β-isomer with a staggered arrangement of the two $SO_3$ groups (both compounds **4a** and **4b** were α-isomers, with an eclipsed arrangement). Both of the fully oxidized clusters were found to exhibit thermochromic behavior unprecedented for discrete POM clusters, changing from pale yellow at 77 K to deep red at 500 K in a fully reversible process (Figure 15.11). This observation, the ~8-nm shift in the HOMO–LUMO centered absorption band, was explained as a consequence of two factors: (a) a slight expansion of the POM framework with increasing temperature, which decreases the LUMO energy, and (b) a broadening of the HOMO energies due to the varying S . . . S distances at higher temperatures [33].

One of the reasons why the fully oxidized disulfite Dawson cluster was thought to be an interesting synthetic target was that the two sulfite clusters could potentially form a bond, leading to the formation of the dithionate $S_2O_6^{2-}$ anion, giving a structure similar to the pyrophosphate Dawson, but without the bridging oxygen atom between the heteroatoms (sulfur is the only main group element which can form an $X_2O_6^{n-}$ ion with an X–X single bond). The formation of the $S_2O_6^{2-}$ is an oxidative process, and it was hoped that stimulating this process could lead to the reduction of the surrounding Dawson cage (a system that was discussed in Section 15.2.4), giving a mixed-valent cage as is found in **4a**. Despite the S . . . S distances in **4a** (3.301(2) Å), **4b** (3.229(2) Å), and **4c** (3.271(5) Å) all being shorter than the sum of the van der Walls radii for two sulfur atoms (~3.6 Å), it appeared that the structural changes required to achieve the ~2.15-Å S–S single bond were too great, and this transformation was not observed in either solid-state or solution phase.

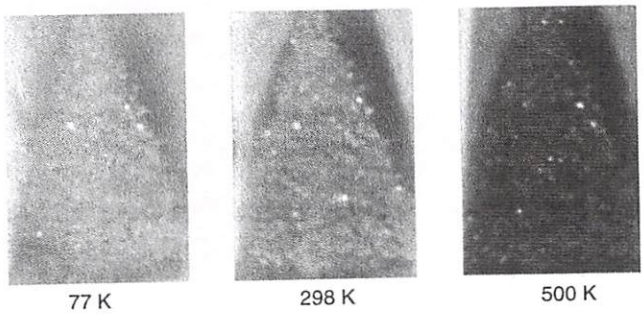


**FIGURE 15.11.** Images showing the changing temperature exhibited by compound **4b**. See color insert.

However, when molecules of **4c**, the staggered β-isomer, were isolated on a gold surface, the formation of the dithionate *was* observed [34]. By radically changing its environment, it became possible to convert the molecule between two distinct electronic states by raising and lowering the temperature. In order to prove the theory that the electrons reducing the metal cage were emanating from the sulfite/dithionate conversion (as opposed to some external source, such as the metal surface), a control cluster $[S_2Mo_{18}O_{62}]^{n-}$ (or $[\{(SO_4)(M_3O_9)_3\}_2]^{n-}$) (**5**) was used. This sulfate Dawson has the same charge as **4c**, its sulfite equivalent, and is actually easier to electrochemically reduce, but the sulfate groups are chemically inert and so cannot provide electrons to the metal cage. Hence, any reduction seen in the sulfite group which is not mirrored in the sulfate group would imply that the reducing electrons must come from the interior of the cluster. This was exactly what was observed when both clusters on a gold surface were analyzed with valence-level photoemission spectroscopy (for the valence-level electronic structure of the cluster layer) and core-level x-ray photoelectron spectroscopy (for the oxidation state of the Mo centers) at both 77 K and 298 K. Compound **5** did not show significant changes with the change in temperature, but the sulfite cluster **4c** showed changes consistent with the proposed reversible intramolecular redox process. The core-level spectrum for **4c** is shown in Figure 15.12, both at 77 K and 298 K, showing the evolution of a shoulder peak at 298 K indicating the presence of $Mo^V$. This shoulder was not observed for compound **5**.

In addition, Figure 15.13 shows the valence-level spectrum showing a band that can be attributed to the Mo $4d^1$ electron, consistent with the core-level spectrum, as well as bands associated with tetrahedral sulfur compounds which appear in the control at both temperatures, but only in the 298 K spectrum for compound **4c**, supporting the hypothesis that the formation of a tetrahedral dithionate-like anion causes the observed reduction of the cage.

In order to understand the effect that the gold surface plays in activating this reaction, density function theory (DFT)

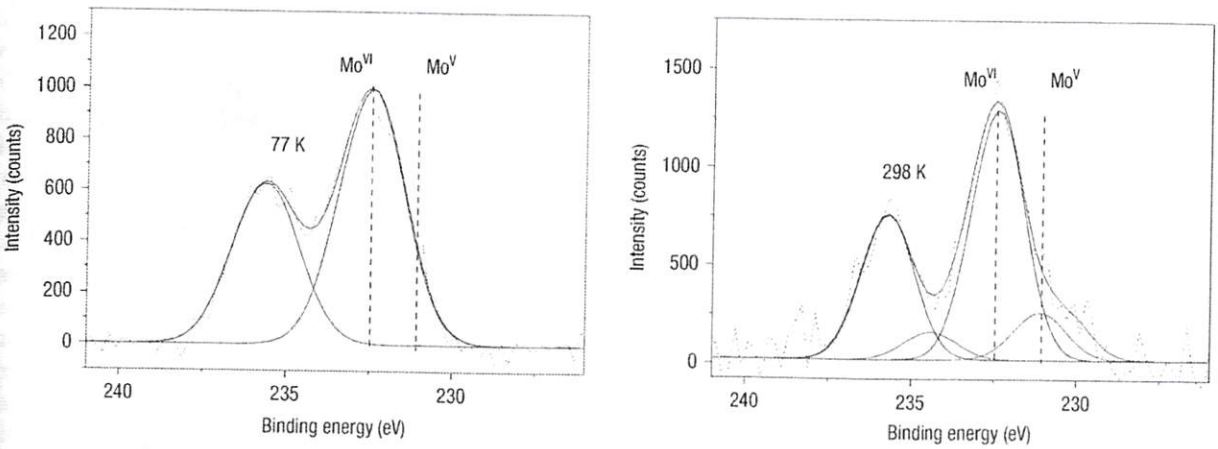


**FIGURE 15.12.** The Mo 3*d* Core-Level Spectra for sulfite Dawson compound **4c** at 77 K and 298 K. At 77 K the observed curve corresponds to the predicted peaks for $Mo^{VI}$, but at 298 K the presence of a shoulder peak at ~230 eV indicates the formation of $Mo^{V}$. The equivalent spectra for the sulfate Dawson do not show the development of this shoulder peak.

calculations were carried out to model the potential electronic effects underpinning the observed electronic changes. Adding a single reaction coordinate by shifting the two S centers of the sulfite Dawson by a displacement $\Delta x$ (to simulate thermal activation) while shifting their oxo ligands by $\Delta x/2$ toward each other (along the main symmetry axis of the cluster), it was found that, in the gas phase, no intramolecular electron transfer nor formation of the S–S bond occurred. However, when the fluctuations in charge density (the *image charge*) induced in the polarizable Au surface by the cluster itself were modeled by four single positive charges forming a rectangle on one arbitrary side of the cluster, the same decrease in S–S distance *did* lead to the formation of a bond and the transfer of electrons to the cage.

Based on this reasoning, the same set of experiments, using both compound **5** and **4c**, were attempted using alternative surfaces: (a) an Au surface coated with a monolayer of cystein and (b) a surface of highly oriented pyrolytic graphite (HOPG). The experiments showed no reaction for either molecule on the cystein-coated Au surface and no reaction for the control on the HOPG. However, compound **4c** on HOPG was found to be in its activated state even at room temperature, and the redox process was irreversible. These results show unambiguously that the surface effect is real: For the untreated gold, the image charges are located within the metal mirror images of their corresponding cluster charges (where the gold surface is the mirror plane), leading to an intermediate stabilization resulting in a reversible formation of the S–S bond with changing temperature; for the cystein-gold surface the image charges are weaker and further away due to the obstruction caused by the cystein molecules, leading to a surface-stabilization too weak to allow S–S bond formation; in contrast to the gold surfaces, however, HOPG localizes the image charges on the surface graphene sheet, bringing them closer to the cluster and increasing the local field felt by the internal S atoms. The effect is sufficiently strong that both $Mo^{V}$ and metallic $Mo^{0}$ species were observed by XPS studies at room temperature, a similar effect having been noted for the untreated gold surface when heated to decomposition at ~500 K. The control molecule did not experience any redox activity for any of the surface experiment, which leads to the remarkable conclusion that the HOPG surface was capable of inducing an internal rearrangement in a POM cluster without directly transferring charge to it (since, if this were the case, the more redox-active sulfate Dawson would also have been reduced).

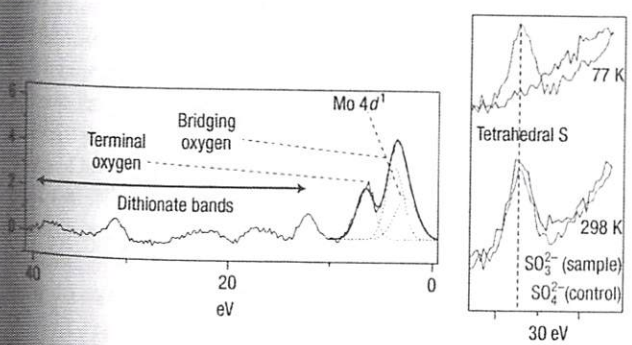


**FIGURE 15.13.** The valence level spectrum for compound **4c**, showing the presence of the Mo $4d^1$ band (**left**) and the change from pyramidal sulfur to tetrahedral sulfur observed for the $SO_3^{2-}$ sample at 298 K (**right**).

After the synthesis of the molybdenum sulfite Dawson, attempts were made to create a tungsten analogue, leading to the formation of two cluster structures [35]: the isostructural equivalent to the molybdenum sulfite cluster, $[W^{VI}{}_{18}O_{54}(SO_3)_2]^{4-}$ (or $[\{(SO_3)(W_3O_9)_3\}_2]^{4-}$) (**6**), and a new

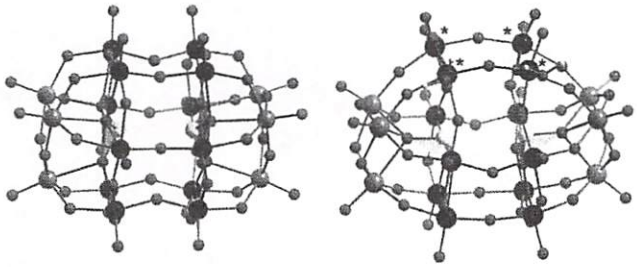

**FIGURE 15.14.** Crystal structures of the W sulfate clusters, with the $[W^{VI}{}_{18}O_{54}(SO_3)_2]^{4-}$ cluster **6** (**left**) and the $[W^{VI}{}_{18}O_{56}(SO_3)_2(H_2O)_2]^{8-}$ cluster **7** (**right**), with the metal centers not bound to the heteroanion indicated by a $*$.

structure, $[W^{VI}{}_{18}O_{56}(SO_3)_2(H_2O)_2]^{8-}$ (or $[\{(SO_3)(W_3O_9)_2(W_3O_{10}(H_2O))\}_2]^{8-}$) (**7**), shown in Figure 15.14.

Structure **7**, in addition to being the first closed *hetero*-POM found to include water ligands, showed some unique electronic properties. In a process similar to the Mo sulfite Dawsons on surfaces, the cluster undergoes an intramolecular redox reaction with the sulfite centers becoming oxidized and the surrounding cluster becoming reduced when the compound is heated to 400°C. However, in contrast to the dithionate formation experienced by the Mo sulfite Dawsons, this reaction involves the oxidation of the sulfite centers to sulfates, involving a rearrangement of the internal oxygens in the POM cage and the loss of the two water ligands, forming a $[W^{VI}{}_{14}W^{V}{}_{4}O_{54}(SO_4)_2]^{8-}$ (**8**) mixed-valence cluster. Although electron-transfer reactions and structural rearrangements are well known for *hetero*-POMs, this was the first example of a reaction combining the two and is also the first example of a fully characterized unimolecular reaction involving a *hetero*-POM.

Structure **7** is capable of this rearrangement due to its unique internal arrangement. Compared to structure **6**, isostructural to the Mo sulfite Dawson, in which the $SO_3$ groups are centrally aligned and each oxygen binds to three of the nine metal centers, in structure **7** the $SO_3$ groups are tilted so that, while one oxygen binds to three metal centers, the remaining two only bind two metal centers. This means that two of the nine metal centers in each half are not bound to the heteroanion, giving a total of four metal centers ($4W^*$) not bound to heteroanions in the cluster which neighbor each other in an equatorial position. These four $W^*$ centers, combined with the tilted sulfite groups, reduce the overall symmetry of the cluster from $D_{3h}$ (as is the case for structure **6**) to $C_{2v}$. The different orientation of the sulfite groups is also represented in the S . . . S distance of 3.61(2) Å, which is significantly longer than the 3.19(1) Å distance in structure **6**. The four $W^*$ metal centers in structure **7** each possess an additional terminal ligand (all metal centers having one terminal oxo ligand to begin with); two of these ligands are terminal oxo ligands ($W^* = O$) while the other two are water ligands. This arrangement results in the bridging oxo ligands between the $W^*$ atoms of each $W_9$ half pointing inwards toward the vacant site of the sulfite groups.

All these factors result in the structure of **7** being essentially prearranged for internal reorganization with a concurrent redox reaction. When heated to 400°C the sulfite groups are oxidized to sulfate, acting as embedded reducing reagents and contributing up to four electrons to the $W_{18}$ cage, leading to the formation of the intense blue mixed-valent cluster **8** with the loss of the two coordinated water ligands from the $W^*$ centers. Since the reduction of the shell is balanced by the oxidation of the heteroanions, the overall charge of the cluster remains constant at 8-.

### 15.3.4 Octahedral Dawson $[(XO_6)M_{18}O_{54}]^{6-}$

***15.3.4.1 Octahedral Heteroatoms ($M_{18}O_{54}(IO_6)$, $M_{18}O_{54}(TeO_6)$).*** The discovery of the $\{W_{19}\}$ *iso*-POM (the Dawson-like structure with an octahedral or trigonal prismatic $WO_6$ template discussed in Section 15.2.5) suggested that it may be possible to form such a structure with an octahedral or trigonal prismatic heteroanion. This led to the synthesis of the $[H_3(IO_6)W_{18}O_{56}]^{6-}$ (or $[(IO_6)(W_3O_9)_4(W_3O_{10})_2(H_3)]^{6-}$) (**9**) cluster, shown in Figure 15.15, as a potassium (**9a**), tetrapropylammonium (TPA) (**9b**), and tetrabutylammonium (TBA) (**9c**) salt. This represents the first example of a Dawson-type cluster templated by an $XO_6$ heteroanion and the first crystallographically characterized tunstatoperiodate [36].

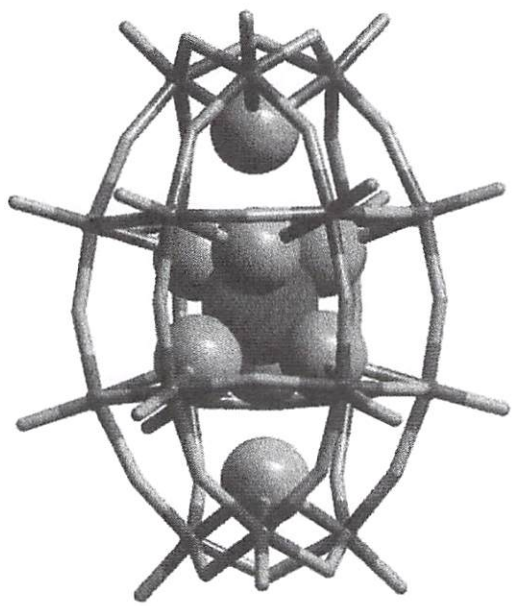

**FIGURE 15.15.** Crystal structure of the $[H_3(IO_6)W_{18}O_{56}]^{6-}$ cluster **9**.

Similar in structure to the $\{W_{19}\}$ cluster, the periodate cluster has two vacant positions where the two conventional heteroanions are usually found and the cap units, normally $[W_3O_9]$, both possess additional oxygen atoms usually provided by the heteroanion, giving $[W_3O_{10}]$. These extra oxygens are either singly or doubly protonated. The main difference between the $\{W_{19}\}$ structure and the periodate is the relative orientation of the cage and the heteroanion: The $D_{3d}$ symmetry of the $IO_6$ anion does not match the $D_{3h}$ symmetry of the cage, resulting in the overall cluster having a $C_{3v}$ symmetry, representing the $\beta^*$ isomer (the first $\beta^*$ Dawson isomer to be identified crystallographically).

Since the only difference between the two clusters is the differing symmetry and the identity of the central heteroatom, it would be exceptionally difficult to confirm by crystallography alone that the supposed periodate cluster was not simply the $\{W_{19}\}$ cluster. In order to confirm the identity of the periodate cluster, high-resolution electrospray and cryospray mass spectrometry (MS) was performed on the **9b** salt and the **9a** salt after cation exchange to give the TPA/K salt, both in acetone, giving a series of peaks that could be attributed to the periodate cluster. This, combined with elemental analysis, confirms the presence of pure cluster **9** without $\{W_{19}\}$ impurities.

Syntheses were attempted for the tellurium analogue of the $[H_3(IO_6)W_{18}O_{56}]^{6-}$ cluster, but conventional synthetic methods did not yield the desired product. Based on the use of mass spectrometry to identify the cluster in the periodate synthesis, a similar procedure was performed on a variety of reaction mixtures, utilizing different cation systems, for the tellurium cluster, revealing peaks corresponding to a tellurium analogue of the periodate Dawson in the dimethylammonium ($DMAH^+$) and tetrabutylammonium (TBA) systems. Crystals were eventually obtained from both these reaction mixtures giving the $[H_3(Te^{VI}O_6)W_{18}O_{56}]^{7-}$ (**10**) cluster as its $DMAH^+$ (**10a**) and TBA (**10b**) salts. This was the first example of tellurium being incorporated into a Dawson-type structure [37].

The structure of cluster **10** is similar to the periodate cluster **9**, except for the symmetry of the two molecules. Cluster **10** adopts the more common $\gamma^*$ conformation in contrast to cluster **9**'s far rarer $\beta^*$ conformation. However, cluster **10** possesses the same voids found in cluster **9** at the sites where the two heteroanions are normally found in the classic Wells–Dawson structure and also shares the additional oxygens found on the caps. Cluster **10** shows some very unusual electronic activity. On exposure in acidified solution to the reducing agent $Na_2S_2O_4$, the usual intense blue colour (stemming from the reduction of W atoms in the cluster shell) was quickly replaced by a pale yellow one. Crystals obtained from this solution showed that a complete internal arrangement had occurred, with a marked shift in the Te position (1.10 Å toward the cap) and the conversion of the octahedral $Te^{VI}O_6$ into the pyramidal $Te^{IV}O_3$ heteroanion, accompanied by the loss of both additional oxygens on the capping triads. This resulted in a final structure of $[H_3(Te^{IV}O_3)W_{18}O_{57}]^{5-}$ (**11**), with a fully oxidized cage, very similar in structure to its Sb analogue $[H_2(Sb^{III}O_3)W_{18}O_{57}]^{7-}$. Both structures can be seen in Figure 15.16.

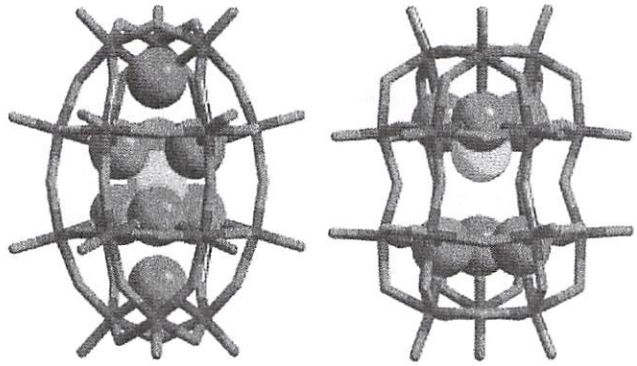

**FIGURE 15.16.** Crystal structures for the $[H_3(Te^{VI}O_6)W_{18}O_{56}]^{7-}$ cluster **10** (**left**) and the product of its reaction with $Na_2S_2O_4$, the $[H_3(Te^{IV}O_3)W_{18}O_{57}]^{5-}$ cluster **11** (**right**).

Further investigations into this rearrangement/redox process showed that by adjusting the pH in solution of the compound to pH 2, nanosized crown-like tetrameric clusters could be formed, consisting of two **11** clusters linked by two $\{W_{11}\}$ units via adjacent distorted W centers on the **11** clusters. This shows that the presence of the pyramidal $Te^{IV}O_3$ heteroanion activates the cage surface to a sufficient extent that it forms nanoscale structures without the addition of other transition metal electrophiles.

## 15.4 THE KEGGIN CLUSTER

While the majority of this chapter is devoted to the Wells–Dawson cluster, since the presence of two internal heteroatoms presents more opportunities for engineering intramolecular reactions, the Keggin clusters have also been incorporated into systems in which its single encapsulated heteroatom plays an important part in the chemical properties of the materials.

### 15.4.1 The Keggin-Net

A great deal of interest has recently been generated in extended modular frameworks incorporating inorganic building blocks [38], such as metal–organic frameworks (MOFs) and coordination polymers [39], which allow for carefully directed assembly of porous structures, and zeolites [40], which offer robust structures with chemical functionality. An ideal system, which combined the controlled assembly of MOFs with the stability and functionality of zeolites and similar systems, would allow for the inclusion of specific

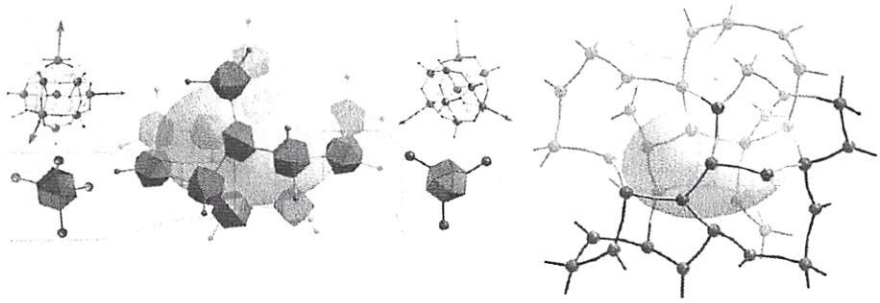

**FIGURE 15.17.** Two representations of the cavities found within the Keggin-net structure. The image on the left emphasizes how the alternating nodes connect around the cavity, while the image on the right emphasizes rings that make up the 3D structure.

guests at "active sites," thereby triggering chemical reactions (e.g., redox reactions) that could switch the nature of the framework. We have already seen that POM structures are highly redox active and that the incorporated heteroatoms in the Keggin and Dawson structures can contribute to this redox activity, so, if a redox active extended modular framework is the goal, one using *hetero*-POM clusters as building blocks would seem like a good synthetic target.

The Keggin-based framework $[(C_4H_{10}NO)_{40}(W_{72}Mn^{III}{}_{12}O_{268}Si_7)_n]$ ($\mathbf{12_{ox}}$), or Keggin-Net, formed from lacunary Keggin clusters $[\gamma\text{-}SiW_{10}O_{36}]$ and $Mn^{II}$ in the presence of morpholinium cations and potassium permanganate, is an example of such a POM-based framework [41]. It is a material that can undergo reversible redox processes; the inclusion of a redox reagent couples with a controlled redox reaction in the framework itself, giving the reduced cluster $\mathbf{12_{red}}$. This reduction occurs at the $Mn^{III}$ heteroatoms, switching these to $Mn^{II}$ and thereby retaining long-range order by cooperative structural changes within the W–O–Mn linkages that connect the Keggin units. Both $\mathbf{12_{ox}}$ and $\mathbf{12_{red}}$ can be dissolved in water and recrystallized to perfectly reform $\mathbf{12_{ox}}$ (with $\mathbf{12_{red}}$ being oxidized upon dissolution). The structure was the first to be formed purely of POM units, without the need for external linkers such as transition metal electrophiles. The lacunary Keggin clusters are linked directly by oxygen bridges between W and Mn atoms (W–O–Mn), and the overall structure is made up of alternating units of trigonal-planar three-linked (connected to three other Keggin units) and tetrahedral four-linked (connected to four other Keggin units) clusters cross-linked into an infinite 3D framework. These can be thought of as an equal distribution of trivacant $\{SiW_9O_{37}\}$ units and tetravacant $(SiW_8O_{36})$ units linked together by W–O–Mn bridges, which fix these units together.

The topology of the framework is identical to that of cubic germanium nitride, $Ge_3N_4$, in which the germanium is equivalent to the tetrahedral nodes and the nitrogen is equivalent to the trigonal nodes [42]. Both structures have puckered eight-membered ellipsoidal rings that are composed of four trigonal and four tetrahedral nodes. For $Ge_3N_4$ the dimensions of the ring are 2.97 Å × 4.61 Å; for the $\mathbf{12_{ox}}$ structure, the equivalent rings have dimensions of 9.45 Å × 12.93 Å, showing the effect of replacing atomic nodes in classic materials with nanosized clusters. Extrapolating the $\mathbf{12_{ox}}$ structure, it may be seen that four of these puckered rings form a larger 3D cavity, as can be seen in Figure 15.17. These cavities have nanoscale dimensions of 2.7 × 2.4 × 1.3 nm and accommodate both the charge balancing cations and a large number of solvent molecules.

Based on the assumption that it should be possible to alter the heteroatom of the $[\gamma\text{-}SiW_{10}O_{36}]$ Keggin unit, a germanium-centered equivalent to the silicon-centerd Keggin-net was produced $[(C_4H_{10}NO)_{40}(W_{72}Mn^{III}{}_{12}O_{268}Ge_7)_n]$ ($\mathbf{13_{ox}}$) [43]. This compound had reactivity very similar to that of compound **12**, with a slightly faster reduction time to $\mathbf{13_{red}}$ and a slower reoxidation time back to $\mathbf{13_{ox}}$. The structural features are also almost identical, with the heteroatom-oxygen distance (1.6 Å for Si–O and 1.75 Å for Ge–O) being the only real distinction, leading to the difference in reactivity of the two frameworks. Adding another level of variability, further work resulted in the synthesis of Keggin-net structures using both Si and Ge heteroatoms, but with cobalt in place of manganese linking the lacunary units together, leading to $[W_{72}Co^{II}{}_{12}O_{268}Si_7]_n$ ($\mathbf{14_{red}}$) and $[W_{72}Co^{II}{}_{12}O_{268}Ge_7]_n$ ($\mathbf{15_{red}}$). In contrast to the Mn structures that crystallized in their 3+ oxidation state and could be reduced to 2+, the Co structures crystallize as 2+ and can be oxidized to 3+. Unlike their Mn counterparts, compounds **14** and **15** are not stable in their modified state and will, if left in solution, reduce back to their native 2+ state.

The availability of these four native structures and their four reduced/oxidized states led somewhat naturally to the idea of forming a framework alloy [44]: a structure based on two different frameworks, A and B, which share the same structure and could be combined to form a framework of AB units, also sharing the same structure. Since the difference in redox activity between the different heteroatoms is slight, the heterometals, Mn and Co, were selected for use, since their redox behavior is completely opposite, one undergoing oxidation while the other undergoes reduction. This was attempted by preparing reaction mixtures of

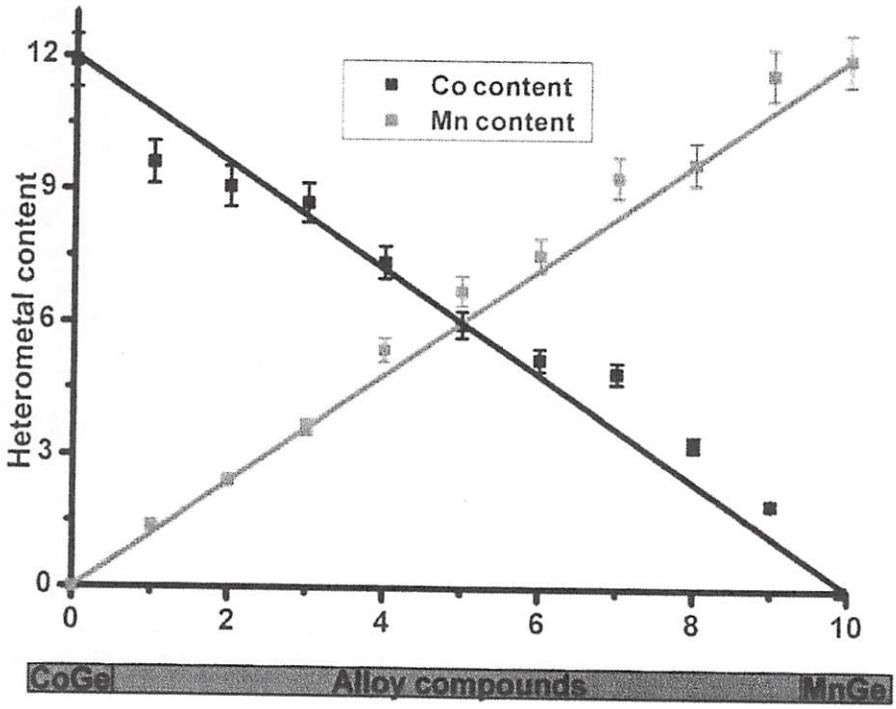


**FIGURE 15.18.** Graph showing the FAAS results for the Co/Mn Keggin-net alloy. It shows that the metal content of the molecular alloys varies linearly with the ratio of the reaction mixtures of **13** and **15**.

$[W_{72}Mn^{III}{}_{12}O_{268}Ge_7]_n$, **13**, and $[W_{72}Co^{II}{}_{12}O_{268}Ge_7]_n$ **14**, using Ge since it gave a far greater yield, and then combining these in varying ratios (9:1, 8:2, etc), resulting in a total of nine different framework alloy compounds. These could be visually identified since they showed a color variant going from the pure $Mn^{III}$ cluster (purple) to the pure $Co^{II}$ cluster (brown). A full spectrum of analysis was performed in order to confirm that the compounds were true alloys and not simply discrete mixtures of single crystals of pure compounds; in particular, flame atomic absorption spectroscopy (FAAS) was used, which confirmed the heterometal content to vary linearly for the 10% Mn/Co mixing steps, as shown in Figure 15.18. Investigations of the 5:5 alloy via cyclic voltammetry showed that the compound possessed some unexpected properties; while the second reduction wave lies at −0.97 V, the intermediate value of the two pure compounds, the first is at −0.893 V, far removed from the intermediate value of −0.76 V.

## 15.5 CONCLUSION

For readers who are unfamiliar with inorganic synthesis but who work extensively with organic capsules, hopefully this will have provided an insight into the possibilities presented by transition metals, both as structural components and as redox active materials. Much current work in POM synthesis focuses on the interface between polyoxometalates and organic structures, developing methods of grafting the two together to form hybrid organic-inorganic structures. The potential that we have seen of these electronically fascinating clusters can be both explored and channeled by extending them with the subtlety and finesse of organic synthesis.

## REFERENCES

1. Vriezema, D. M., Comellas Aragonès, M., Elemans, J. A. A. W., Cornelissen, J. J. L. M., Rowan, A. E., Nolte, R. J. M. (2005). Self-assembled nanoreactors. *Chemical Reviews*, **105**(4), 1445–1490.
2. Leininger, S., Olenyuk, B., Stang, P. J. (2000). Self-assembly of discrete cyclic nanostructures mediated by transition metals. *Chemical Reviews*, **100**(3), 853–908.
3. (a) Caulder, D. L., Powers, R. E., Parac, T. N., Raymond, K. N. (1998). The self-assembly of a predesigned tetrahedral $M_4L_6$ supramolecular cluster. *Angewandte Chemie International Edition*, **37**(13–14), 1840–1843. (b) Davis, A. V., Fiedler, D., Ziegler, M., Terpin, A., Raymond, K. N. (2007). Resolution of chiral, tetrahedral $M_4L_6$ metal ligand hosts. *Journal of the American Chemical Society*, **129**(49), 15354–15363. (c) Davis, A. V., Raymond, K. N. (2005). The big squeeze: guest exchange in an $M_4L_6$ supramolecular host. *Journal of the American Chemical Society*, **127**(21), 7912–7919. (d) Pluth, M. D., Johnson, D. W., Szigethy, G. Z., Davis, A. V., Teat, S. J., Oliver, A. G., Bergman, R. G., Raymond, K. N. (2008). Structural consequences of anionic host–cationic guest interactions in a supramolecular assembly. *Inorganic Chemistry*, **48**(1), 111–120.
4. (a) Brumaghim, J. L., Michels, M., Pagliero, D., Raymond, Kenneth N. (2004). Encapsulation and stabilization of

reactive aromatic diazonium ions and the tropylium ion within a supramolecular host. *European Journal of Organic Chemistry*, **2004**(24), 5115–5118. (b) Brumaghim, J. L., Michels, M., Raymond, Kenneth N. (2004). Hydrophobic chemistry in aqueous solution: Stabilization and stereoselective encapsulation of phosphonium guests in a supramolecular host. *European Journal of Organic Chemistry*, **2004**(22), 4552–4559. (c) Dong, V. M., Fiedler, D., Carl, B., Bergman, R. G., Raymond, K. N. (2006). Molecular recognition and stabilization of iminium ions in water. *Journal of the American Chemical Society*, **128**(45), 14464–14465.

5. Pluth, M. D., Bergman, R. G., Raymond, K. N. (2007). Making amines strong bases: Thermodynamic stabilization of protonated guests in a highly-charged supramolecular host. *Journal of the American Chemical Society*, **129**(37), 11459–11467.
6. Kirby, A. J. (1994). Enzyme mimics. *Angewandte Chemie International Edition*, **33**(5), 551–553.
7. (a) Pluth, M. D., Bergman, R. G., Raymond, K. N. (2007). Acid catalysis in basic solution: A supramolecular host promotes orthoformate hydrolysis. *Science*, **316**(5821), 85–88. (b) Pluth, M. D., Bergman, R. G., Raymond, K. N. (2008). Supramolecular catalysis of orthoformate hydrolysis in basic solution. *Journal of the American Chemical Society*, **130**(34), 11423–11429.
8. (a) Pluth, M. D., Bergman, R. G., Raymond, K. N. (2007). Catalytic deprotection of acetals in basic solution with a self-assembled supramolecular "nanozyme". *Angewandte Chemie International Edition*, **46**(45), 8587–8589. (b) Pluth, M. D., Bergman, R. G., Raymond, K. N. (2008). The acid hydrolysis mechanism of acetals catalysed by a supramolecular assembly in basic solution. *The Journal of Organic Chemistry*, **74**(1), 58–63.
9. Radzicka, A., Wolfenden, R. (1995). A proficient enzyme. *Science*, **267**(5194), 90–93.
10. Hastings, C. J., Pluth, M. D., Bergman, R. G., Raymond, K. N. (2010). Enzyme-like catalysis of the nazarov cyclization by supramolecular encapsulation. *Journal of the American Chemical Society*, **132**(20), 6938–6940.
11. Kohlschütter, V., Tüscher, J. L. (1920). Zur Kenntnis topochemischer Reaktionen. Uber Bildung und Verhalten von Kupferhydroxyd. *Zeitschrift für anorganische und allgemeine Chemie*, **111**(1), 193–236.
12. Fujita, M., Oguro, D., Miyazawa, M., Oka, H., Yamaguchi, K., Ogura, K. (1995). Self-assembly of ten molecules into nanometer-sized organic host frameworks. *Nature*, **378**(6556), 469–471.
13. Yoshizawa, M., Takeyama, Y., Kusukawa, T., Fujita, M. (2002). Cavity-directed, highly stereoselective [2 + 2] photodimerization of olefins within self-assembled coordination cages. *Angewandte Chemie International Edition*, **41**(8), 1347–1349.
14. Takaoka, K., Kawano, M., Ozeki, T., Fujita, M. (2006). Crystallographic observation of an olefin photodimerization reaction that takes place via thermal tumbling within a self-assembled host. *Chemical Communications*, (15), 1625–1627.
15. Kawano, M., Kobayashi, Y., Ozeki, T., Fujita, M. (2006). Direct crystallographic observation of a coordinatively unsaturated transition-metal complex in situ generated within a self-assembled cage. *Journal of the American Chemical Society*, **128**(20), 6558–6559.
16. Pope, M. T. (1983). *Heteropoly and Isopoly Oxometalates*, Vol. 8. Springer-Verlag, Berlin.
17. (a) Miras, H. N., Cooper, G. J. T., Long, D.-L., Bogge, H., Müller, A., Streb, C., Cronin, L. (2010). Unveiling the transient template in the self-assembly of a molecular oxide nanowheel. *Science*, **327**(5961), 72–74. (b) Long, D.-L., Abbas, H., Kögerler, P., Cronin, L. (2004). A high-nuclearity "Celtic-ring" isopolyoxotungstate, $[H_{12}W_{36}O_{120}]^{12-}$, that captures trace potassium ions. *Journal of the American Chemical Society*, **126**(43), 13880–13881. (c) Müller, A., Kögerler, P., Dress, A. W. M. (2001). Giant metal-oxide-based spheres and their topology: From pentagonal building blocks to keplerates and unusual spin systems. *Coordination Chemical Reviews*, **222**, 193–218. (d) Xu, F., Scullion, R. A., Yan, J., Miras, H. N., Busche, C., Scandurra, A., Pignataro, B., Long, D.-L., Cronin, L. (2011). A supramolecular heteropolyoxopalladate $\{Pd_{15}\}$ cluster host encapsulating a $\{Pd_2\}$ dinuclear guest: $[Pd^{II}{}_2\{H_7Pd^{II}{}_{15}O_{10}(PO_4)_{10}\}]^{9-}$. *Journal of the American Chemical Society*, **133**(13), 4684–4686.
18. (a) Kepert, D. L. (2007). *Isopolytungstates in Progress in Inorganic Chemistry*. John Wiley & Sons, Hoboken, NJ, pp. 199–274. (b) Tytko, K.-H., Glemser, O. (1976) Isopolymolybdates and isopolytungstates. In: Emeléus, H. J., Sharpe, A. G., eds. *Advances in Inorganic Chemistry*, Academic Press, Vol. 19, pp. 239–315.
19. Vilà-Nadal, L., Rodriguez-Fortea, A., Yan, L. K., Wilson, E. F., Cronin, L., Poblet, J. M. (2009). Nucleation mechanisms of molecular oxides: A study of the assembly-dissassembly of $[W_6O_{19}]^{2-}$ by theory and mass spectrometry. *Angewandte Chemie International Edition*, **48**(30), 5452–5456.
20. (a) Müller, A., Kögerler, P., Kuhlmann, C. (1999). A variety of combinatorially linkable units as disposition: From a giant icosahedral keplerate to multi-oxide based network structures. *Chemical Communications*, (15), 1347–1358. (b) Cronin, L., Kögerler, P., Müller, A. (2000). Controlling growth of novel solid-state materials via discreet molybdenum-oxide-based building blocks as synthons. *Journal of Solid State Chemistry*, **152**(1), 57–67. (c) Cronin, L., Beugholt, C., Krickemeyer, E., Schmidtmann, M., Bögge, H., Kögerler, P., Luong, T. K. K., Müller, A. (2002). "Molecular symmetry breakers" generating metal-oxide-based nano-object fragments as synthons for complex structures: $[\{Mo_{128}Eu_4O_{388}H_{10}(H_2O)_{81}\}_2]^{20-}$], a giant-cluster dimer. *Angewandte Chemie International Edition*, **41**(15), 2805–2808.
21. Song, Y.-F., Long, D.-L., Ritchie, C., Cronin, L. (2011). Nanoscale polyoxometalate-based inorganic/organic hybrids. *The Chemical Record*, **11**(3), 158–171.
22. Abbas, H., Pickering, A. L., Long, D.-L., Kögerler, P., Cronin, L. (2005). Controllable growth of chains and grids from polyoxomolybdate building blocks linked by silver(I) dimers. *Chemistry—A European Journal*, **11**(4), 1071–1078.
23. Lewis, D. W., Willock, D. J., Catlow, C. R. A., Thomas, J. M., Hutchings, G. J. (1996). De novo design of

structure-directing agents for the synthesis of microporous solids. *Nature*, **382**(6592), 604–606.

24. Ritchie, C., Burkholder, E. M., Long, D.-L., Adam, D., Kögerler, P., Cronin, L. (2007). Exploiting the multifunctionality of organocations in the assembly of hybrid polyoxometalate clusters and networks. *Chemical Communications*, (5), 468–470.
25. (a) Long, D.-L., Abbas, H., Kögerler, P., Cronin, L. (2004). A high-nuclearity "Celtic-ring" isopolyoxotungstate, $[H_{12}W_{36}O_{120}]^{12-}$, that captures trace potassium ions. *Journal of the American Chemical Society*, **126**(43), 13880–13881. (b) Long, D.-L., Brücher, O., Streb, C., Cronin, L. (2006). Inorganic crown: The host–guest chemistry of a high nuclearity "celtic-ring" isopolyoxotungstate $[H_{12}W_{36}O_{120}]^{12-}$. *Dalton Transactions*, (23), 2852–2860. (c) Streb, C., McGlone, T., Brücher, O., Long, D.-L., Cronin, L. (2008). Hybrid host–guest complexes: Directing the supramolecular structure through secondary host-guest interactions. *Chemistry—A European Journal*, **14**(29), 8861–8868. (d) McGlone, T., Streb, C., Long, D.-L., Cronin, L. (2009). Guest-directed supramolecular architectures of $\{W_{36}\}$ polyoxometalate crowns. *Chemistry—An Asian Journal*, **4**(10), 1612–1618.
26. Long, D.-L., Kögerler, P., Parenty, A. D. C., Fielden, J., Cronin, L. (2006). Discovery of a family of isopolyoxotungstates $[H_4W_{19}O_{62}]^{6-}$: Encapsulating a $\{WO_6\}$ moiety within a $\{W_{18}\}$ Dawson-like cluster cage. *Angewandte Chemie International Edition*, **45**(29), 4798–4803.
27. Contant, R., Thouvenot, R. (1993). A reinvestigation of isomerism in the dawson structure: Syntheses and $^{183}W$ NMR structural characterisation of three new polyoxotungstates $[X_2W_{18}O_{62}]^{6-}$ (X = PV, AsV). *Inorganica Chimica Acta*, **212**(1–2), 41–50.
28. Jeannin, Y., Martin-Frere, J. (1979). X-ray study of $(NH_4)_7[H_2AsW_{18}O_{60}]\cdot 16H_2O$: First example of a heteropolyanion containing protons and arsenic(III). *Inorganic Chemistry*, **18**(11), 3010–3014.
29. Ozawa, Y., Sasaki, Y. (1987). Synthesis and crystal structure of $[(CH_3)_4N]_6[H_3BiW_{18}O_{60}]$. *Chemical Letters*, 923–926.
30. Himeno, S., Saito, A., Hori, T. (1990). Synthesis and characterization of 18-molybdopyrophosphate complex. *Bulletin of the Chemical Society of Japan*, **63**, 1602.
31. Kortz, U., Pope, M. T. (1994). Polyoxometalate–diphosphate complexes. 2. Structure of 18-molybdopyrophosphate, $[(P_2O_7)Mo_{18}O_{54}]^{4-}$, which encloses a linear, eclipsed conformation of the pyrophosphate anions, and preliminary characterization of Its one- and two-electron heteropoly blues. *Inorganic Chemistry*, **33**(25), 5643–5646.
32. Long, D.-L., Kögerler, P., Cronin, L. (2004). Old clusters with new tricks: Engineering S–S interactions and novel physical properties in sulfite-based dawson clusters. *Angewandte Chemie International Edition*, **43**(14), 1817–1820.
33. Tsunashima, R., Long, D.-L., Endo, T., Noro, S.-I., Akutagawa, T., Nakamura, T., Cabrera, R. Q., McMillan, P. F., Kögerler, P., Cronin, L. (2011). Exploring the termochromism of sulfite-embedded polyoxometalate capsules. *Physical Chemistry Chemical Physics*, **13**(16), 7295–7297.
34. Fleming, C., Long, D. L., Mcmillan, N., Johnston, J., Bovet, N., Dhanak, V., Gadegaard, N., Kögerler, P., Cronin, L., Kadodwala, M. (2008). Reversible electron-transfer reactions within a nanoscale metal-oxide cage mediated by metallic substrates. *Nature Nanotechnology*, **3**(4), 229–233.
35. (a) Long, D.-L., Abbas, H., Kögerler, P., Cronin, L. (2005). Confined electron-transfer reactions within a molecular metal-oxide "trojan horse". *Angewandte Chemie International Edition*, **44**(22), 3415–3419. (b) Cabrera, R. Q., Long, D.-L., Cronin, L., McMillan, P. F. (2010). In situ investigations of the polyoxometalate trojan horse compound $K_7Na[(W^{VI}{}_{18}O_{56}(SO_3)_2(H_2O)_2]\cdot 20H_2O$ under high temperature and high pressure conditions. *CrystEngComm*, **12**(9), 2568–2572.
36. Long, D.-L., Song, Y. F., Wilson, E. F., Kögerler, P., Guo, S. X., Bond, A. M., Hargreaves, J. S. J., Cronin, L. (2008). Capture of periodate in a $\{W_{18}O_{54}\}$ cluster cage yielding a catalytically active polyoxometalate $[H_3W_{18}O_{56}(IO_6)]^{(6-)}$ embedded with high-valent iodine. *Angewandte Chemie International Edition*, **47**(23), 4384–4387.
37. Yan, J., Long, D.-L., Wilson, E. F., Cronin, L. (2009). Discovery of heteroatom-"embedded" Te subset of $\{W_{18}O_{54}\}$ nanofunctional polyoxometalates by use of cryospray mass spectrometry. *Angewandte Chemie International Edition*, **48**(24), 4376–4380.
38. Chae, H. K., Siberio-Pérez, D. Y., Kim, J., Go, Y., Eddaoudi, M., Matzger, A. J., O'Keeffe, M., Yaghi, O. M. (2004). A route to high surface area, porostiy and inclusion of large molecules in crystals. *Nature*, **427**(6974), 523–527.
39. (a) Serre, C., Mellot-Draznieks, C., Surblé, S., Audebrand, N., Filinchuk, Y., Férey, G. (2007). Role of solvent–host interactions that lead to very large swelling of hybrid frameworks. *Science*, **315**(5820), 1828–1831. (b) Hasegawa, S., Horike, S., Matsuda, R., Furukawa, S., Mochizuki, K., Kinoshita, Y., Kitagawa, S. (2007). Three-dimensional porous coordination polymer functionalized with amide groups based on tridentate ligand: Selective sorption and catalysis. *Journal of the American Chemical Society*, **129**(9), 2607–2614.
40. Yuan, H.-M., Chen, J.-S., Zhu, G.-S., Li, J.-Y., Yu, J.-H., Yang, G.-D., Xu, R.-R. (2000). The first organo-templated cobalt phosphate with a zeolite topology. *Inorganic Chemistry*, **39**(7), 1476–1479.
41. Ritchie, C. I., Streb, C., Thiel, J., Mitchell, S. G., Miras, H. N., Long, D.-L., Boyd, T., Peacock, R. D., McGlone, T., Cronin, L. (2008). Reversible redox reactions in an extended polyoxometalate framework solid. *Angewandte Chemie International Edition*, **47**(36), 6881–6884.
42. Kroll, P. (2003) *J. SolidState Chem.*, **176**, 530–537.
43. Thiel, J., Ritchie, C., Streb, C., Long, D.-L., Cronin, L. (2009). Heteroatom-controlled kinetics of switchable polyoxometalate frameworks. *Journal of the American Chemical Society*, **131**(12), 4180–4181.
44. Thiel, J., Ritchie, C., Miras, H. N., Streb, C., Mitchell, S. G., Boyd, T., Ochoa, M. N. C., Rosnes, M. H., McIvet, J., Long, D.-L., Cronin, L. (2010). *Angewandte Chemie International Edition*, **49**(39), 6984–6988.